A population balance model for the flow-induced preparation of Pickering emulsions

A population balance model for the flow-induced preparation of Pickering emulsions

Graziano Frungieri*, Heiko Briesen

Chair of Process Systems Engineering, TUM School of Life Sciences, Technical University of Munich, Gregor-Mendel-Straße 4, 85354 Freising, Germany

Abstract

In this work we studied the flow-induced preparation of oil-in-water Pickering emulsions by means of a bivariate population balance model. We characterized oil droplets by their size and surface coverage by solid particles, and we took into account all phenomena responsible for their change, namely coalescence and breakup of the droplets, and particle-droplet collisions leading to surface coverage. We studied the population dynamics in a uniform shear flow and in a turbulent flow field, and stabilization was observed in both cases. Under shear, the population evolved by coalescence phenomena, which, together with particle adsorption, led to a prompt and full stabilization of the emulsion droplets. An inverse scaling between particle load and droplets Sauter diameter was found, and seen to well compare with previously reported experimental data. In turbulence, stabilization was also obtained. In this case, the droplet size evolved through a peculiar path, showing a size undershoot before equilibrium conditions were reached. We explained this as a consequence of the coalescence phenomena, that alongside breakup, affected the transient of the process. Results shed a new light onto the dynamics of preparation of Pickering emulsions and aim at constituting a reference for the set-up and interpretation of experiments.

Keywords: breakup, coalescence, droplet coverage, Monte Carlo, Pickering emulsions, population balance model, size stabilization

1. Introduction

Pickering emulsions are emulsions in which the droplets of the disperse phase are stabilized against coalescence by a shell of adsorbed solid particles (Ngai & Bon, 2014). These systems have

*Corresponding author
Email address: graziano.frungieri@tum.de (Graziano Frungieri)

recently gained popularity because solid particles have displayed a superior ability, compared to molecular surfactant, in stabilizing emulsions (Aveyard et al., 2003). This can be explained *i*) by the extremely high free energy barrier that adsorbed particles must overcome to detach from the liquid-liquid interface – which makes particle adsorption practically irreversible (Binks, 2002) – and *ii*) by the steric hindrance constituted by adsorbed particles which prevent droplets to come into close proximity, thus preventing coalescence (Frijters et al., 2014; Binks & Lumsdon, 2000).

The use of solid particles in liquid-liquid emulsions is not new (Ramsden, 1904; Pickering, 1907), but only recently it became of special interest to a number of key industries and in a range of applications (Low et al., 2020). In the food industry, for instance, the use of solid stabilizers derived from plants (e.g. cellulose nanofibrils, soy protein particles or starch granules) can be expected to replace the traditionally used chemically-synthesized and animal-derived surfactants (Lv et al., 2021; López-Pedrouso et al., 2022; Jing et al., 2022; Guo et al., 2022; Frungieri et al., 2022b; Ferrari et al., 2022). In the pharmaceutical industry, particle covered droplets, also referred to as *colloidosome*, are promising for their potential use as drug carriers with tuned release profiles of the active ingredient (Wang et al., 2021; Sharkawy et al., 2021; Vasquez Giuliano et al., 2022b,a), and in chemical catalysis, particle covered droplets have shown both hetero and homogeneous catalytic properties (Voisin et al., 2021; Zhang et al., 2019; Zhao et al., 2021; Chang et al., 2021).

Despite the growing interest, the production of Pickering emulsions is still fraught with several challenges and it is mainly still based on empirically derived protocols, with a limited number of works (Tsabet & Fradette, 2015; Kempin et al., 2020) that have specifically addressed the effect of the processing conditions on the emulsion final properties. The mechanism by which Pickering emulsions are formed under a fluid flow should be expected to be indeed complex and determined by several concurrent phenomena: during processing, droplets in fact undergo coverage due to the solid particle attachment to their surface (Hajisharifi et al., 2021, 2022), and they change in size as a result of the flow-induced coalescence and breakup phenomena. A pioneering work in this regard was conducted by Arditty et al. (2003) who prepared o/w (oil-in-water) emulsions stabilized by amphiphilic nanometric silica particles. Following a simple lab protocol, samples of the oil-water-particles mixture were vigorously mixed by hand, the kinetic evolution of the droplet size was optically followed, and, at equilibrium, an inverse proportionality between droplet size and amount of dispersed solid particles was observed. By means of three-dimensional lattice Boltzmann simulations, Frijters et al. (2014) observed the

same inverse dependence between particle concentration and size of the stabilized droplets. On the droplet scale phenomena, Fan & Striolo (2012), by dissipative particle dynamics simulations, investigated the mechanism of coalescence between particle-covered droplets, and observed that the particles packing density on the droplets surface is the most important parameter determining the occurrence of coalescence. Similar conclusions were drawn by Pawar et al. (2011) by experimental tests. The deformation and breakup of particle-covered droplets under fluid dynamic stresses has also been investigated. Luo & Bai (2020) studied the motion of a particle-covered droplet flowing through a microchannel and showed that particles jam in the rear of droplet and induce a nearly complete immobilization of its surface. Similarly, Mei et al. (2016) reported that, at large surface coverage, a percolated network of contacting particle forms on the droplet surface, suppressing both deformation and breakup.

Coalescence, breakup and the particle adsorption phenomena on the droplet surface are size-dependent processes, thus making the preparation of Pickering emulsions strongly affected by the droplet population polydispersity. For this reason, we see a population balance model (PBM) as the just framework for gaining more in-depth insights into the process. Population balance models are able to track, over a population of dispersed entities, the evolution of one or more properties of interest (such as size, shape, bulk or surface composition) by modeling all the physical phenomena which may be responsible for their change (such as surface growth, coagulation, breakup, bulk or interfacial reactions). Thus, PBMs have been employed over the years for the most diverse uses, including the characterization of crystallization processes (Briesen, 2006), the processing of conventional emulsions (Lebaz et al., 2021; Solsvik et al., 2014), the dynamics of gas-liquid flows (Maluta et al., 2021, 2022; Niño et al., 2020), and particle synthesis, dissolution, aggregation and breakup phenomena (Para et al., 2022; Zhao et al., 2018; Frungieri et al., 2020b, 2022a). Even problems from social science have been investigated by means of population balances (Kuhn et al., 2018) and, in the context of heteroaggregation, with which the processing of Pickering emulsions shares several common features, a number of problems of practical relevance have been studied. These include, among others, the clustering occurring in mixtures of particles with different zeta potential (Rollié et al., 2009; Chaturbedi et al., 2016; Frungieri et al., 2020a), the aggregation between air bubbles and microorganism in dissolved air flotation equipment (Schmideder et al., 2018) or the aggregation between magnetic particles and suspended solids occurring in magnetic seeded separation processes (Ge et al., 2015; Rhein et al., 2019). Finally, in the more specific realm of Pickering emulsions, a population balance model has been recently devised by Siva & Ho (2022) to study an ultrasound-based

synthesis route.

In the present work we studied the production of Pickering emulsions as determined by the action of an externally imposed flow field. We addressed the case of a shear-induced coalescence process and of a turbulent emulsification. In both cases we characterized the population of droplets by using two internal characterizing variables, namely droplet size and droplet degree of coverage by solid particles. We took into account all phenomena responsible for their change, including droplet-droplet coalescence, droplet breakup and droplet-particle collisions. We used established literature models for describing collision and breakup frequencies, whereas novel models for describing coalescence and breakup efficiencies were formulated. These were based on the most recent findings about the mechanism of such processes for particle-covered droplets. We opted for a stochastic event-driven Monte Carlo algorithm for solving the formulated population balance model (Frungieri & Vanni, 2017, 2021; Singh et al., 2022). Results elucidated the mechanism by which Pickering emulsions are formed in a fluid flow and offered several insights into the process, which can be possibly used for setting up processing routes with predictable kinetics and emulsion final properties.

The paper is organised as follows: in Section 2, we report on the developed Monte Carlo algorithm for studying Pickering emulsion processing in both a laminar shear and a turbulent flow. Results, focused on the characterization of the transient of the process and on the equilibrium properties of the emulsions, are discussed in Section 3, concluding remarks follow in Section 4.

2. Methodology

We studied the preparation of Pickering emulsions in a flow field starting from a pre-formed emulsion composed of micrometric oil droplets, coexisting in water together with nanometric solid particles. We described the population of droplets by two internal characterizing variables, namely the droplet radius R and the surface coverage by solid particles, denoted as ϕ in the following. No internal variables were needed to describe the population of solid particles, which was assumed to be monodisperse and stable against aggregation.

We tracked the droplets population dynamics in a subvolume, assuming that its behavior replicates the statistical features of a real emulsion as a whole. Two different scenarios were studied: in the first, a fine emulsion (droplet initial radius equal to 10μm) evolves in a uniform shear flow. This kind of flow field is for instance the one encountered in cone-plate cells or the one that, in spatially non-uniform flow fields, can be observed at least locally at the scale of the

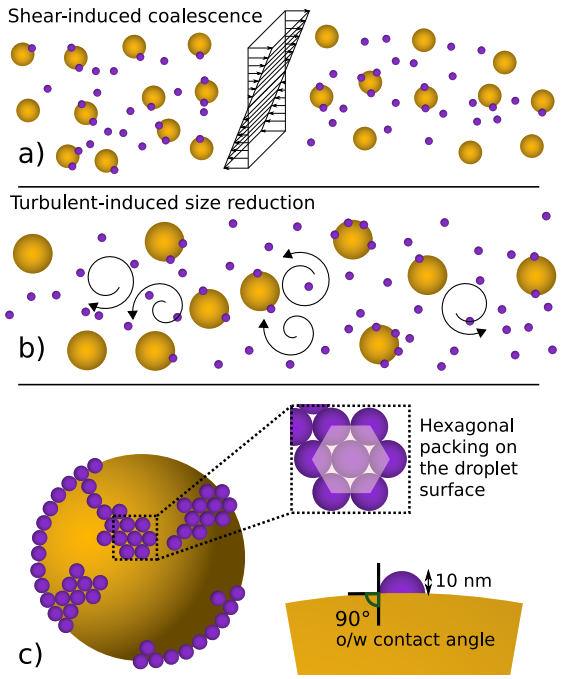

Figure 1: Illustration of the two investigated scenarios for producing an oil-in-water Pickering emulsion. a) Shear-induced coalescence of a fine pre-emulsion (initial droplet radius = 10 μm). b) Turbulence induced size reduction in a coarser pre-emulsion (initial droplet radius = 50 μm). In both cases two internal variables were used to describe the droplets, namely size and surface coverage by solid particles. We started all our simulations from a population of droplets with zero surface coverage. All particles were therefore initially dispersed in the water bulk phase. c) Schematics of the solid particles arrangement on the droplet surface.

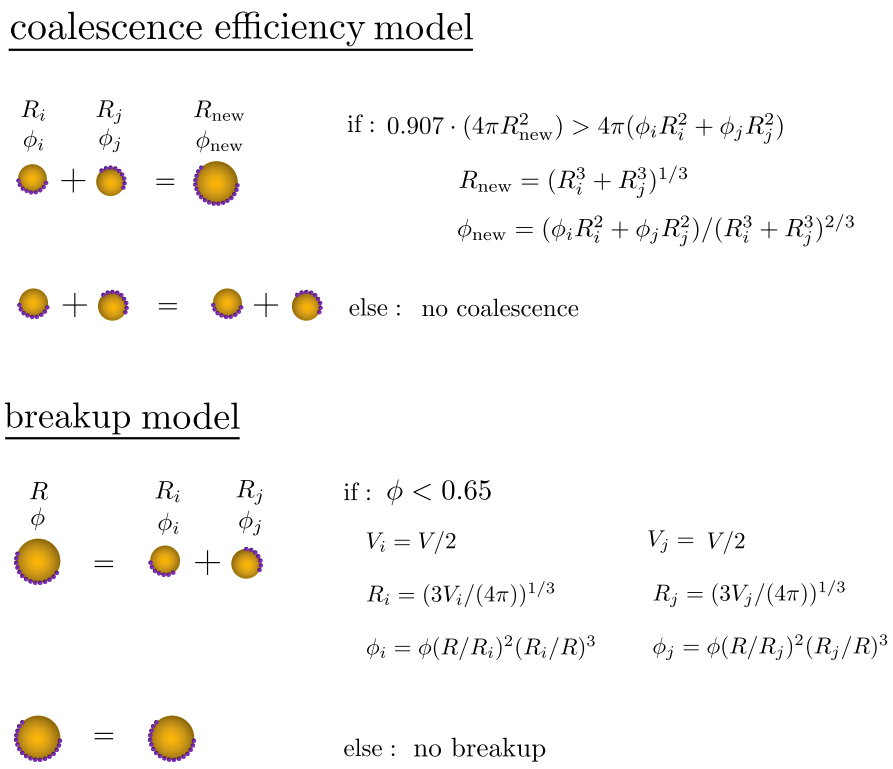

Figure 2: Model for the coalescence and breakup efficiencies. Coalescence and breakup frequencies were calculated according to the characteristics of the investigated flow.

droplets. In the second scenario, a coarser population of droplets (droplet radius equal to 50 μm) is dispersed in an isotropic and homogeneous turbulent flow. This flow field can be safely assumed to hold at the droplets scale and macroscopically, for sufficiently intense turbulence, it can be for instance observed in the bulk of large stirred tanks, where boundary layer effects are negligible. Figure 1a) and b) depict graphically the two investigated cases.

The solid particles had equal affinity towards the aqueous and oil phase, such that upon collision with the oil droplets they adsorbed irreversibly, sitting at the oil-water interface with a contact angle that we assumed to be equal to 90° (Fig. 1c). We postulated that the particles adjust themselves on the droplet surface according to a hexagonal packing scheme. For such an arrangement, the maximum attainable packing fraction on a planar surface is 0.907. In our simulations, given the large size disproportion between the droplets (10-2000 μm) and the solid particles (10 nm), we assumed this limit to hold true despite the actually spherical shape of our interfaces. Furthermore, we assumed particles to form at most a monolayer on the droplet surface and to not form aggregates protruding in either bulk of the two phases.

As it will be discussed later, we computed the rate of droplet collision and breakup using established models (Coulaloglou & Tavlarides, 1977; Smoluchowski, 1918; Solsvik et al., 2013; Alopaeus et al., 2002), whereas a new model for describing the effectiveness of such processes was devised based on the recent literature for particle-covered droplets. Pawar et al. (2011) have experimentally shown that, when partially covered droplets come into close proximity, particles placed in the contact region are displaced towards the periphery, where they accumulate forming concentric ring structures. This allows the liquid phase of the droplets to come into contact and coalescence to occur. However, depending on the droplets coverage fraction, the outcome of the encounter varies. When the droplets surface coverage is small, full coalescence, leading to the formation of a new spherical droplet, occurs. On the contrary, when the droplet surface coverage is large, coalescence is prevented, as the particle crowding effect on the droplet surface hinders the particle motion. Also intermediate cases, leading to the generation of complex not-spherical shaped droplets, were reported and explained as consequence of a balance between the anisotropic Laplace stress distribution within the arrested shape and the elastic reaction of the particle-jammed interface (Pawar et al., 2011). We opted for including these observations in our numerical modelling, limiting ourselves, however, to consider the two extreme outcomes only, namely the full coalescence and the total prevention of coalescence. In Fig. 2 (top) the coalescence efficiency model we derived upon is depicted and reported. Full coalescence occurs whenever two colliding droplets would result into a droplet whose surface coverage being lower than the maximum attainable one ($\phi_{\max} = 0.907$). No coalescence takes place in other case.

Breakup occurs in a fluid flow as soon as droplets experience a mechanical stress that overcomes their internal resistance. This may happen either because the droplet size grows over a critical threshold, or because droplets, as they move through the flow, experience regions of large hydrodynamic stress. The first situation is relevant in uniform flows, such as the case of a laminar shear flow. Both are instead relevant in spatially and/or time varying flow fields, such as a turbulent flow. In both situations, as shown in Fig. 2 (bottom), we assumed that upon breakup two droplets with equal size are produced. Such an assumption is dictated by the lack in the literature of any other established model describing the fragment size distribution for particle-covered droplets. Following the recent literature, we assumed, however, that over the percolation limit (surface coverage $\phi \approx 0.65$), solid particles have adjusted themselves into a network of contacting particles, which makes the droplet behave as a *hard sphere* with infinite resistance to breakup. This strengthening effect induced by the adsorbed solid particles has been recently reported in Gai et al. (2017) and Mei et al. (2016).

2.1. Population dynamics in laminar shear flow

We described the frequency of the encounter between two spherical droplets with radii R_i and R_j as (Smoluchowski, 1918):

$$f_{\mathrm{enc}}\left(R_i, R_j\right) = \frac{4}{3}\frac{\dot{\gamma}}{V}\left(R_i + R_j\right)^3 \tag{1}$$

where $\dot{\gamma}$ is the shear flow intensity, and where V is the volume of the simulated sample. From Eq. (1) the total encounter frequency in the sample follows as $f_{\mathrm{enc,tot}} = \sum_i^{n_D-1}\sum_{j=i+1}^{n_D} f_{i,j}$ where n_D is the number of droplets considered in the Monte-Carlo scheme and where for the sake of conciseness $f_{i,j} = f_{\mathrm{enc}}\left(R_i, R_j\right)$. Equation (1) only describes the frequency of encounters between droplets. The outcome of the encounter was assessed according to the efficiency model of Fig. 2. In a uniform shear, if droplets grow over a critical size, they undergo breakup. The occurrence of breakup was assessed by the droplet capillary number $Ca = \mu_w\dot{\gamma}R_i/\sigma$, where μ_w is the dispersing medium viscosity, $\dot{\gamma}$ is the shear rate intensity, and σ the interfacial tension. Above a critical capillary number which only depends on the ratio between the disperse and dispersing phase viscosities μ_o/μ_w (Debruijn, 1991; Grace, 1982), a droplet will eventually break up, and, as already stated, we assumed this would lead to the generation of two equally sized droplets.

Droplets, besides coalescence and breakup phenomena, experience a progressive covering as a result of the collisions and irreversible adsorption of the solid particles on their surface. We assumed this to occur as a result of both the shear-induced collisions between oil droplets and particles, and of the Brownian motion of the solid particles. Therefore, for a droplet of radius R_i the rate of coverage read as:

$$\dot{\phi}(R_i) = \left(\frac{4}{3}\dot{\gamma}(R_i + a)^3 + 4\pi\mathcal{D}\left(R_i + a\right)\right)\left(\frac{a}{2R_i}\right)^2 c_{\mathrm{pcle}}\Gamma_i \tag{2}$$

where a is the particle radius, $\mathcal{D}$ is the particle diffusivity, computed as $k_BT/(6\pi\mu_w a)$, and where Γ_i is a droplet-particle attachment efficiency, linearly decreasing with the droplet instantaneous coverage. It is defined as:

$$\Gamma_i\left(\phi\right) = \left(1 - \frac{\phi}{\phi_{\max}}\right) \tag{3}$$

and it is equal to zero at the maximum surface coverage $\phi_{\max} = 0.907$.

In Eq. (2), c_{pcle} is the instantaneous number concentration of solid particles dispersed in the continuous phase. This was updated throughout the simulation as:

$$\frac{dc_{\mathrm{pcle}}}{dt} = -\sum_i^{n_d}\left(\frac{4}{3}\dot{\gamma}\left(R_i + a\right)^3\frac{1}{V} + 4\pi\mathcal{D}\left(R_i + a\right)\frac{1}{V}\right)c_{\mathrm{pcle}}\Gamma_i \tag{4}$$

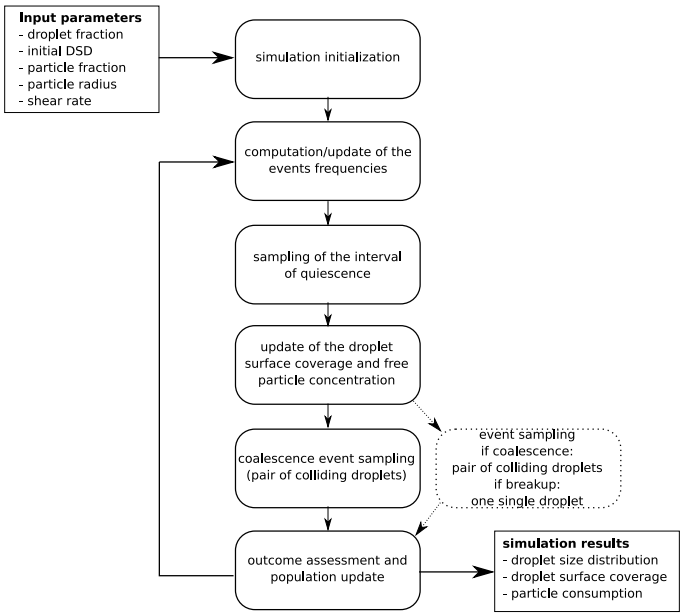

Figure 3: Flowchart of the Monte Carlo algorithm used to solve the droplet population dynamics in shear flow. The dotted box represents the algorithm as modified to model the population dynamics in turbulence, where coalescence and breakup occur simultaneously at their own frequency. Simulations were conducted using a number of simulated droplets ranging between 3750 and 7500.

where one can again distinguish the contribution due to shear and the one due to the particle Brownian motion. Note that several orders of magnitude separate the particle and the droplet radius, and that our simulations were run at a shear rate intensity large enough to make the rate of particle attachment by shear largely dominating over the Brownian one. Under this condition, from Eq. (2), it can be inferred that larger droplets, because of their larger capture section, undergo a faster coverage compared to the smaller ones. Furthermore, this leads to a few scaling features of our model at varying shear and solid particle radius. Interested readers are referred to the Supplementary Material of this article for such considerations.

2.2. Numerical algorithm

In Fig. 3 we illustrate the algorithm used for solving the population dynamics. We resorted to a Monte Carlo (MC) algorithm based on the event-driven technique and interval of quiescence concept put forth by Kendall (1949) and Shah et al. (1977). From the total encounter frequency of the system, an interval of quiescence (Δt) can be estimated (Shah et al., 1977). The interval of quiescence has to be intended as a time interval during which no encounter between droplets occurs, the droplet size does not change, and the population only undergoes surface coverage.

Table 1: Physical parameters of the shear-induced coalescence simulations. R is the droplet radius, σ the oil/water interfacial tension, a the particle radius, μ_w and μ_o the water and oil density, respectively. The maximum coverage is $\phi_{\max}$, the adopted shear rate intensity is $\dot{\gamma}$. The droplet critical capillary number was calculated as in Debruijn (1991). See the Supplementary material for a discussion about the scaling features of the model.

R	σ	a	μ_w	μ_o	oil fraction	$\phi_{\max}$	$\dot{\gamma}$	Ca_{cr}
μm	mN/m	nm	Pa·s	Pa·s	v/v %	-	s^{-1}	-
10-3000	30	10	10^{-3}	$3 \cdot 10^{-3}$	0.1	0.907	1000	2.17

The following cumulative distribution function was adopted to sample stochastically the Δt elapsing between two subsequent encounter events (Shah et al., 1977):

$$F(\Delta t) = 1 - \exp(-f_{\text{enc,tot}} \cdot \Delta t) \tag{5}$$

where $f_{\text{enc,tot}}$ is the total encounter frequency in the sample.

The MC also sampled the droplets involved in an encounter event: after computing the encounter frequencies relative to all the possible binary encounters (Eq. (1)), by picking a random number ξ from a uniform distribution between 0 and 1, the sampled event was the one with index q which satisfied the following relationship:

$$\sum_{k=1}^{q-1} f_{ij|k} < f_{\text{tot}} \cdot \xi < \sum_{k=1}^{q} f_{ij|k} \tag{6}$$

where q could assume any value from 1 to $n_D(n_D-1)/2$, with n_D being the number of droplets in the sample.

The physical parameters of the investigated systems are reported in Table 1. Further details about the MC algorithm, and about its implementation can be retrieved in Frungieri & Vanni (2021) and in Frungieri et al. (2020a). A validation of the implemented algorithm by a comparison with the solution obtained by a sectional method is reported in the Supplementary Material of this article.

2.3. Droplet dynamics in turbulence

Few modifications to the Monte Carlo algorithm are needed to address the droplet population dynamics in a turbulent flow. Contrarily to the case of a uniform shear, in a turbulent flow droplet coalescence and breakup occur simultaneously, with the first being determined by the rate of droplet-droplet collisions and the second by the rate of droplets entering high

energy turbulent eddies. Assuming that the turbulence is isotropic and that the droplet size lies in the inertial subrange, we described the droplet-droplet encounter frequency according to (Coulaloglou & Tavlarides, 1977):

$$f_{\mathrm{enc}}(D_i, D_j) = c_0 \frac{\varepsilon^{1/3}}{V} (D_i + D_j)^2 \left(D_i^{2/3} + D_j^{2/3} \right)^{1/2} \tag{7}$$

with D_i and D_j being the droplet diameters and ε being the turbulent dissipation rate, assumed to be uniform in the sample. From Eq. (7) the total encounter frequency reads as $f_{\mathrm{enc,tot}} = \sum_i \sum_{j=i+1} f_{\mathrm{enc}}(i,j)$.

Turbulence is also responsible for droplet breakup. We compute the droplet breakup frequency according to (Alopaeus et al., 2002):

$$f_{\mathrm{brk}}(D_i) = C_1 \varepsilon^{1/3} \mathrm{erfc} \left(\sqrt{\frac{C_2 \sigma}{\rho_w \varepsilon^{2/3} D_i^{2/3}} + \frac{C_3 \mu_o}{\sqrt{\rho_w \rho_o} \varepsilon^{1/3} D_i^{4/3}}} \right) \tag{8}$$

where ρ_w and ρ_o are the water and oil density, respectively, and where σ is the oil-water surface tension. From Eq. (8) the total breakup frequency in the system follows as $f_{\mathrm{brk,tot}} = \sum_i^{n_D} f_{i,\mathrm{brk}}$.

Since coalescence and breakup occur simultaneously, each at the frequency determined by the flow statistics, the MC algorithm was in this case in charge of also sampling the kind of expected event. This was done according to the relative probability of occurrence of each event, with the probability of collision given by $P_{\mathrm{enc}} = f_{\mathrm{enc,tot}}/(f_{\mathrm{enc,tot}} + f_{\mathrm{brk,tot}})$ and similarly the one of breakup (Lee & Matsoukas, 2000). When a breakup event was sampled, the involved droplet was chosen by picking a random number ξ from a uniform distribution between 0 and 1, and the chosen event was the one with index q which satisfied the following relationship:

$$\sum_{k=1}^{q-1} f_{i,\mathrm{brk}|k} < f_{\mathrm{brk,tot}} \cdot \xi < \sum_{k=1}^{q} f_{i,\mathrm{brk}|k} \tag{9}$$

where q could assume any value from 1 to n_D, with n_D being the number of droplets in the sample. In case a collision event was sampled, the relationship reported in Eq. (6) was used for determining the pair of colliding droplets.

The rate of surface coverage of the droplets was computed as:

$$\dot{\phi}(R_i) = \left(c_0 \varepsilon^{1/3} (D_i + 2a)^2 \left(D_i^{2/3} + (2a)^{2/3} \right)^{1/2} \right) \left(\frac{a}{D_i} \right)^2 c_{\mathrm{pcle}} \Gamma_i \tag{10}$$

where the attachment efficiency $\Gamma = \Gamma(\phi)$ reads as in Eq. (3). Analogously to Eq. (4), from Eq. (10) the total rate of particle adsorption can be derived. We did not include in this case the contribution of the Brownian motion in the rate of particle attachment, as this was seen

Table 2: Set of parameters used for the turbulent induced preparation of Pickering emulsions. Surface tension, particle radius, viscosities and droplet volume fraction read as in Table 1. The parameters of the coalescence and breakup frequency fall in the ranges typically reported for turbulent emulsification in stirred vessels. (Alopaeus et al., 2002; Maluta et al., 2021)

Parameter	Symbol	Value
Turbulent dissipation rate	ε	40 $\mathrm{m}^2\ \mathrm{s}^{-3}$
Initial droplet diameter	D	100 μm
Minimum droplet diameter	$D_{\min}$	10 μm
oil density	ρ_o	1000 $\mathrm{kg} \cdot \mathrm{m}^{-3}$
water density	ρ_w	1000 $\mathrm{kg} \cdot \mathrm{m}^{-3}$
coalescence kernel parameter	C_0	1.0
breakup kernel parameter	C_1	10.0
breakup kernel parameter	C_2	$7.75 \cdot 10^{-4}$
breakup kernel parameter	C_3	0.20

to be largely negligible under the conditions of turbulence investigated. The set of parameters used for studying the population dynamics in turbulence is reported in Table 2, whereas the overall simulation flowchart is illustrated in Fig. 3 by small modifications to the algorithm used for addressing the population dynamics in uniform shear.

As coalescence and breakup events takes place in the emulsion, the number of simulated droplets changes over time. When coalescence prevails, the number of simulated droplets decreases. To ensure the statistical robustness of our results, we adjusted the size of the simulated volume throughout the simulation. Whenever the number of simulated droplets fell below a threshold value (set equal to 3/4 of its initial value), the volume of the sample was doubled and every droplet cloned, preserving the droplet volume fraction, the droplet size distribution and the particle concentration (Liffman, 1992). When breakup prevails, the number of simulated droplets may increase up to the point of making computations extremely slow. To tackle this, we opted for randomly halving the population and consequently adjusting the volume of the sample, whenever the number of simulated droplets increased over 1.5 times its initial value. This approach, contrarily to what happens when doubling the system, inevitably introduces a disturbance in the statistics of the droplet distribution (Maisels et al., 2004); however, this was seen to be negligible in our setup. All simulations were run using a number of simulated droplets ranging between 3750 and 7500. A convergence study at varying initial number of simulated

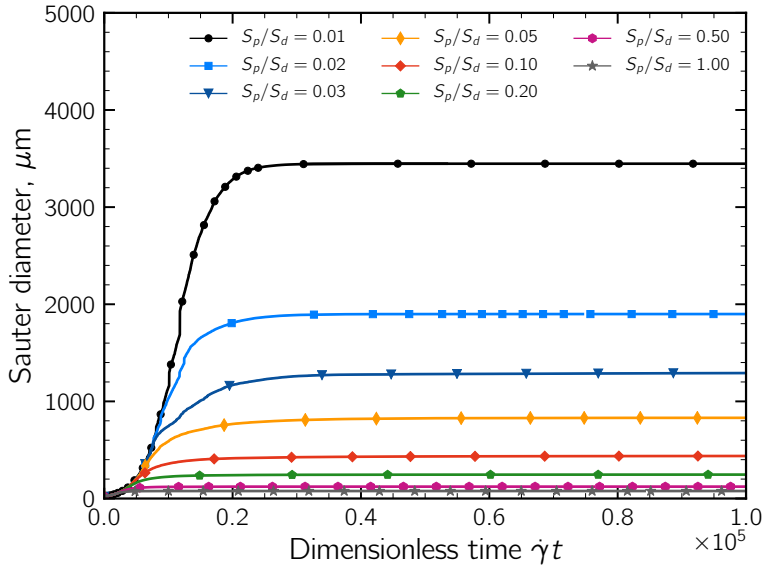

Figure 4: Temporal evolution of the Sauter diameter of the droplet population at varying particle content. We measured the particle content by the ratio at time zero between the total particle surface S_p and the total droplet surface S_d. Time was made dimensionless by the shear rate intensity. Markers are used to ease the reading of the graph and do not indicate the time-resolution with which the model was solved.

droplets is reported in the Supplementary Material of this article.

3. Results

3.1. Pickering emulsions by shear-induced coalescence

We analyzed a model system composed of a population of oil droplets with radius equal to 10μm, dispersed in water at a fraction of 0.1% v/v. The water phase was loaded with a monodisperse population of solid particles with radius equal to 10 nm. We studied the kinetics of coalescence under shear at varying concentration of solid particles. We characterized the different emulsions by making use of the ratio S_p/S_d, which was computed, at time zero, as the ratio between the total particle surface S_p and the total droplet surface S_d. Recalling that solid particles attach at the oil-water interface with a contact angle of 90°, each covering a circular area given by $1/2 \cdot 4\pi a^2$, with a being the particle radius, an initial S_p/S_d ratio equal to $1/2 \cdot \phi_{\max}$ indicates that solid particles are dispersed in an amount in principle able to cover the whole droplet population. However, the change in size of the droplets due to the occurrence of coalescence and breakup phenomena does not allow one to draw in advance such predictions.

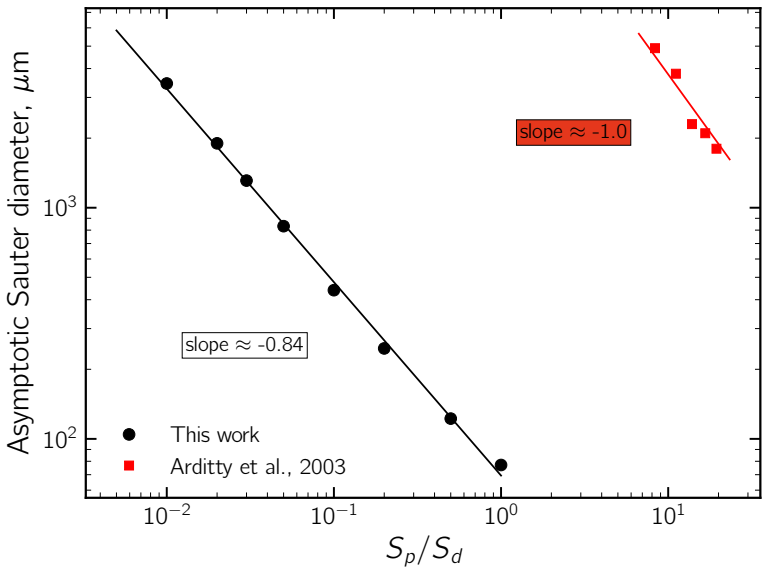

Figure 5: Power-law relationship between the equilibrium droplet Sauter diameter and amount of solid particles originally dispersed in the sample. The red data have been extracted from the work by Arditty et al. (2003).

In Fig. 4 we report, at varying S_p/S_d ratio, the droplet Sauter diameter $D_{3,2} = \sum_i^{N_d} D_i^3 / \sum_i^{N_d} D_i^2$ as a function of time. It can be observed that after a growing phase, the droplet Sauter diameter attained an asymptotic value in all investigated emulsions. As during the process no breakup phenomena were observed, this behavior has to be considered a consequence of the progressive coverage of the droplets by solid particles, which reduced the coalescence efficiency in the emulsions over time. Macroscopically, we noticed that the droplets Sauter diameter at equilibrium scales inversely with the particle content.

In Fig. 5 we report the asymptotic droplet Sauter diameter of the different emulsions as function of the amount of solid particles dispersed in the system. The plot also reports experimental data extracted from the work by Arditty et al. (2003), who investigated coalescence in a similar Pickering o/w emulsion. However, few differences hold between the protocols adopted in our and their case. In Arditty et al. (2003) very concentrated (90 % v/v) and coarse o/w emulsions were prepared by handshaking and the droplet size distribution was tracked during resting. Therefore, in their work, coalescence occurred between oil droplets that were permanently in contact with each other, and over whose surface supposedly the solid particles had been already adsorbed before coalescence started to affect the system. In our case, on the contrary, coalescence was induced by shearing a free-surface emulsion, and droplet coverage by solid particles and coalescence occurred simultaneously until size stabilization was reached. Due to the lack

of the necessary details in the protocol, we did not try to actually simulate the experimental case investigated in Arditty et al. (2003). Nevertheless, we observed that the data scale very similarly, both decaying as the concentration of solid particles is increased. We explain the small discrepancy in the scaling exponent as the consequence of the different droplet size distributions at equilibrium. In Arditty et al. (2003) very narrow distributions were found for all investigated particle concentrations, and indeed a linear scaling should hold in such a case (Wiley, 1954). Our droplet size distributions, as it will be later discussed, are more scattered and showed a stronger dependence on the particle content.

Figure 6 reports the temporal evolution of the droplet average coverage. As the droplet dynamics was governed by coalescence events, each leading to a reduction of the interfacial area, the droplet coverage showed, as expected, a monotonous increase over time. However, its growth dynamics strongly depended upon the amount of solid particles. When the particle concentration was low (see for instance the curve for $S_p/S_d = 0.02$), the surface coverage curve presented a peculiar sigmoidal shape: in this system, initially the increase of the surface coverage is dominated by the particle-droplet collisions (which occurred at a small rate, given the low particle content) and by coalescence between poorly covered droplets. As coalescence proceeded, new larger droplets, with a degree of surface coverage larger than the parents one, were formed. These, because of their larger size, were preferably involved in other coalescence events (see Eq. (1)), thus they further grew and promptly increased their surface coverage, mostly by coalescence and in particular at the expenses of the smaller, less covered droplets. Finally, in a rather short time, all droplets became completely or nearly completely covered (cfr. curves at $S_p/S_d = 0.01$ and 0.02 in Fig. 6).

For larger amounts of solid particles ($S_p/S_d \approx 0.03-0.20$) we did not observe this fast growing coverage regime. Here, given the larger concentration of solid particles, the droplet average coverage reached in a quite short time rather high values, thus inducing also an early reduction of the coalescence efficiency. Therefore, in this systems, coalescence was sooner halted, and the coverage kept increasing as a consequence solely of the collisions between droplets and free particles, which determined a progressive and slower coverage dynamics. In this concentration range, the maximum packing was reached in the more loaded systems ($S_p/S_d \approx 0.10 - 0.20$), but it was not in the particle poor ones ($S_p/S_d \approx 0.03 - 0.05$).

At even larger amounts of solid particles ($S_p/S_d > 0.20$) the average coverage grew very rapidly and soon reached the maximum allowed value. In this concentration range, coalescence events were halted in the very early stage of the process, thus the coverage increased solely by

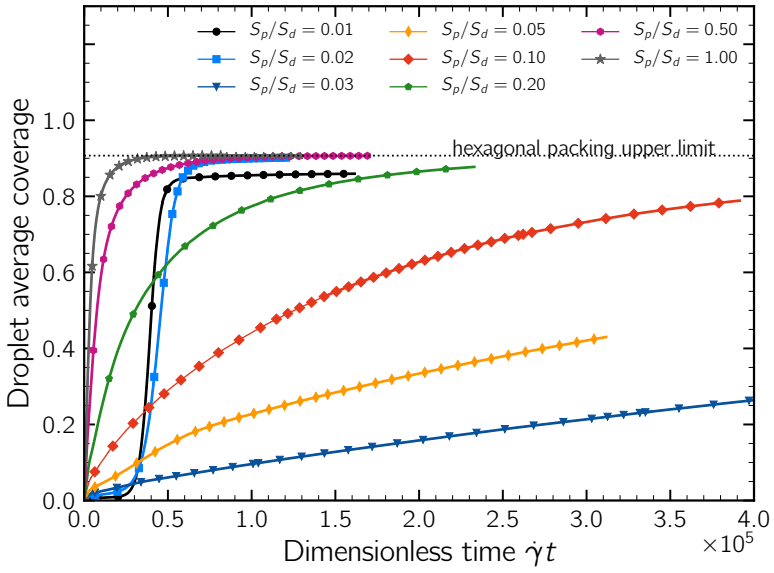

Figure 6: Temporal evolution of the average coverage of the droplet population at varying particle content, measured by the ratio between the total particle surface S_p and the total droplet surface S_d at time zero.

droplet-particle collisions, which, given the large amount of solid particles, proceeded fast and induced a prompt and full coverage.

In Fig. 7 we report the population bivariate distributions at varying particle content. Each data point in the plots reports the droplet diameter and coverage of the droplets after size stabilization was reached; the corresponding monovariate (integrally projected) numerical distributions are reported on the sides in a histogram representation. At low particle concentration ($S_p/S_d = 0.02$) both size and coverage distributions are very narrow. In this system, droplets have the largest possible degree of surface coverage ($= 0.907$) and are large (diameter ≈ 2000 μm). This size distribution, even if attained in the presence of a very small amount of solid particles, is very different from the one that would have been obtained at a zero particle concentration. In a pure emulsion in fact, shear favors the coalescence between the largest droplets. This, provided that breakup does not affect the system, eventually would lead to the formation of few giant droplets and, on a longer time scale, to the complete separation of the two phases. Here, even if the amount of solid particles was small, we observed a completely different behavior. As already discussed, large droplets, because of the large degree of coverage they generally had, did not coalesce among themselves, but they grew incorporating the smaller and less covered ones. This finally led at equilibrium to a completely stabilized population of droplets with a narrow distribution in both size and coverage.

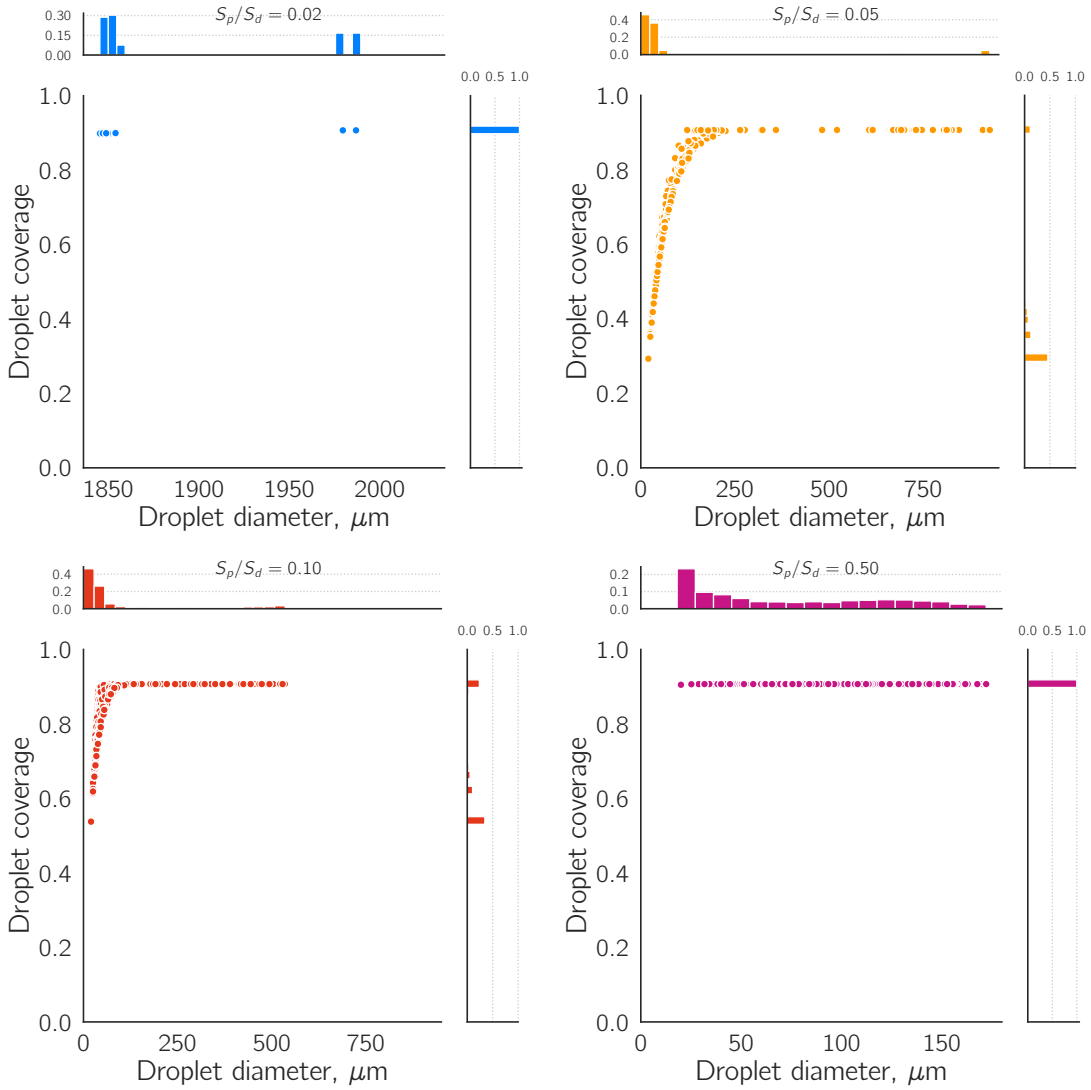

Figure 7: Bivariate size-coverage distribution at varying particle content. Each data point reports the diameter and coverage of the droplets as detected after size equilibrium conditions were reached. Populations are typically composed of a number of droplets between 3750 and 7500. The data points of droplets with identical or similar properties overlap each other. Please notice that different size ranges were used for the abscissa axis.

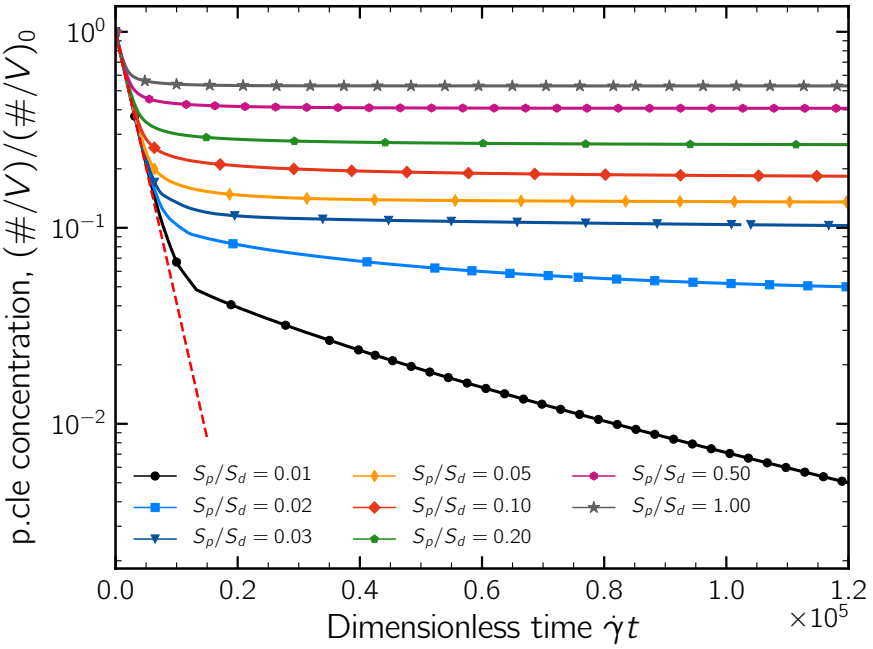

Figure 8: Temporal evolution of the free particle concentration at varying particle content. All curves in the initial stage of the process collapse onto one single curve of the kind $\exp(-kt)$ and reported as a red dashed line in the graph. Compared to the previous graphs, the time range is here restricted to the initial stage of the process.

At intermediate S_p/S_d ratio (= 0.05-0.10) the distributions are scattered both in size and surface coverage. Here, the larger amount of solid particles led to an early drop of the coalescence efficiency, which halted coalescence and froze the size distribution after a rather short time. This caused the formation of few large droplets with a high degree of surface coverage and a large amount of smaller ones with a surface coverage rather far from the maximum attainable value. Nevertheless, coverage was already large enough to hinder further growth.

As the amount of solid particles was further increased, distributions again became narrow both in size and coverage (see the graph for $S_p/S_d = 0.50$) In this case, a large coverage was promptly attained, thus freezing the size distribution in the very early stage of growth, preventing the formation of large droplets.

Finally, Fig. 8 reports the numerical concentration of free particles as a function of time, normalized by the initial concentration. After normalization, for short times, the particle concentration decays exponentially in all emulsions. Revisiting Eq. 4, this is not unexpected, as in all systems, initially all droplets had a bare surface and the overall attachment efficiency was

equal to unity. Hence, the particle consumption rate goes as $dc_{\mathrm{pcle}}/dt \propto -c_{\mathrm{pcle}}$. However, as droplet coverage proceeded, the attachment efficiency linearly decreased, and approached zero at the maximum coverage. This early suppressed particle adsorption in the most particle-rich emulsions here investigated ($S_p/S_d \geq 0.5$) and substantially dampened the rate of particle adsorption in the less loaded ones, especially in those having intermediate particle concentrations ($S_p/S_d = 0.05 - 0.20$), in which the population at equilibrium was composed by a large number of small droplets, undergoing slow coverage. Finally, it is interesting to note that the particle concentration went practically to zero in the particle-poor systems ($S_p/S_d < 0.02$) and nevertheless full coverage was obtained, whereas a large amount of particles was left in the more loaded emulsions. This observation, combined with previous results, suggests that upon carefully selecting the particle load, a balance between extent of particle adsorption, size of the droplets and surface coverage can be found. In our view, this makes shear-induced coalescence an attractive route for the controlled preparation Pickering emulsions.

3.2. Pickering emulsions by turbulence

The second route we investigated for producing Pickering emulsions made use of a pre-emulsion of oil droplets with diameter equal to 100μm and of a homogeneous and isotropic turbulent flow field. As in the previous case, we investigated the scenario in which droplets all have an initial bare surface, and we focused our analysis on the effect of the particle concentration on the process kinetics and size and coverage distributions at equilibrium.

Figure 9 reports the temporal evolution of the Sauter diameter of the oil droplets for varying amount of solid particles. Under the investigated conditions, turbulence yielded reduction of the droplet size. Therefore, compared to the previous shear-induced coalescence case, larger amounts of solid particles were here needed to stabilize the emulsions. When no solid particles were present (curve $S_p/S_d = 0.00$), droplet breakup prevailed over coalescence in the initial stage of the process, but at a later stage, coalescence and breakup balanced each other and the average droplet size attained a constant value. A similar behavior could be observed at small particle concentrations (see curves for $S_p/S_d = 0.05$ and 0.5), whereas in the more particle-loaded emulsions ($S_p/S_d = 2.50$) a distinctive undershoot in the Sauter diameter emerged. In this system, droplets underwent simultaneously size reduction and extensive coverage. The first should be in principle expected to lead to a reduction of the average coverage. However, the large amount of solid particles dispersed counteracted this effect and made droplets attaining a large surface coverage in quite a short time. Then, as soon as the surface coverage of the droplets

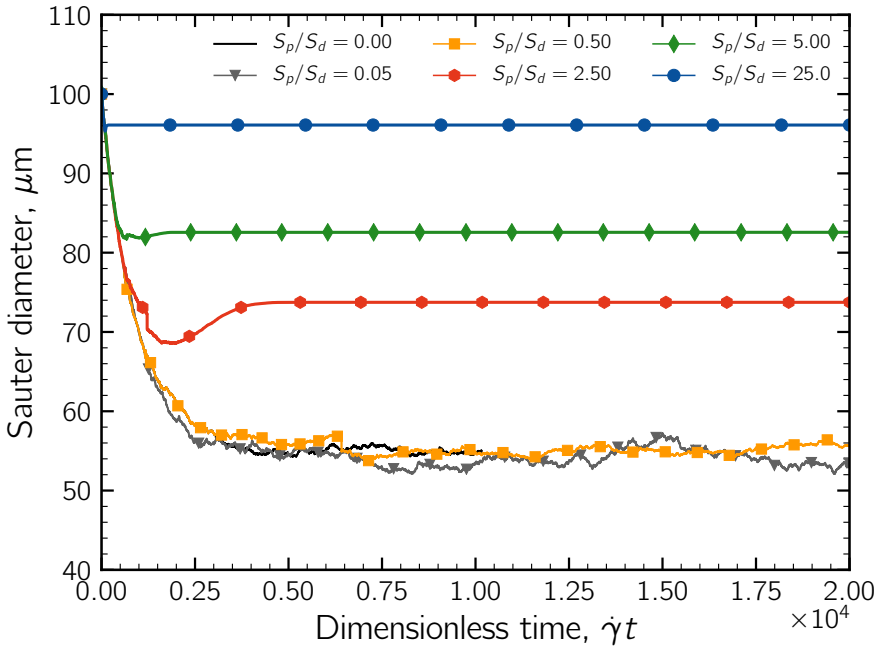

Figure 9: Temporal evolution of the Sauter diameter of the droplet population at varying initial ratio between the total particle surface S_p and the total droplet surface S_d. The time scale has been made dimensionless by an equivalent shear rate $\dot{\gamma}$ computed as $\sqrt{\varepsilon/\nu}$, with ν being the water phase kinematic viscosity.

reached the percolation limit (= 0.65), droplets became invulnerable to breakup and therefore, they could only be possibly involved in coalescence events. This is the reason why the Sauter diameter reached a minimum temporary size, and then increased again. Finally, as coverage proceeded further, also coalescence was halted and the droplet size attained its asymptotic value. This peculiar behavior is particularly visible for $S_p/S_d = 2.50$ but it affected the size dynamics also at larger particle contents.

In Fig. 10 we report the droplet coverage (panel a) and the particle bulk concentration (panel b) as a function of time. It is apparent in particular in the emulsions containing an intermediate amount of solid particles ($S_p/S_d = 2.50$) that the droplet coverage (panel a) increased quickly in the initial stage of the process and slowed down afterwards, presenting two non-stationary inflections points: the first one roughly corresponding to the switch between the breakup-dominated and the coalescence-dominated phase occurring around $\dot{\gamma}t = 0.125 \cdot 10^4$, and the second, at $\dot{\gamma}t \approx 0.35 \cdot 10^4$, corresponding to the suppression of coalescence and to the onset of a final covering regime controlled by particle-droplet collisions only. At equilibrium, as shown in panel b, a substantial amount of solid particles was left in the continuous phase ($\approx 50\%$ of the initial content).

At larger particle content, ($S_p/S_d \geq 5.00$) the coverage kinetics was instead rapid, droplets soon reached the maximum coverage (panel a), both breakup and coalescence were soon prevented, and a large amount of particles was found in the emulsion after size stabilization was attained (panel b).

At low particle content ($S_p/S_d = 0.05$ and 0.5), particles are totally consumed at steady state (panel b), but the droplet population did not reach a surface coverage large enough to resist both coalescence and breakup (see the asymptotic average $\phi \approx 0.15$ at $S_p/S_d = 0.50$, rather far from the percolation limit), thus explaining why, at low particle concentrations, the size dynamics reported in Fig. 9 did not differ from the one of a pure, particle-free emulsion.

Finally, we present in Fig. 11 the size and coverage distributions that we observed in the emulsions after equilibrium conditions were reached. In the particle-poor emulsion ($S_p/S_d = 0.50$) the droplet population at equilibrium is composed by a large amount of small droplets (diameter $< 50\mu m$) with a low surface coverage (< 0.2), which coexist with few, fully covered large droplets with a diameter which is larger than the initial one. The presence of this latter class of droplets is a clear indication that alongside breakup, coalescence played a key role in the emulsification transient and led to the formation of droplets with a large degree of surface coverage, which, once reached the percolation limit, could not be broken down anymore by

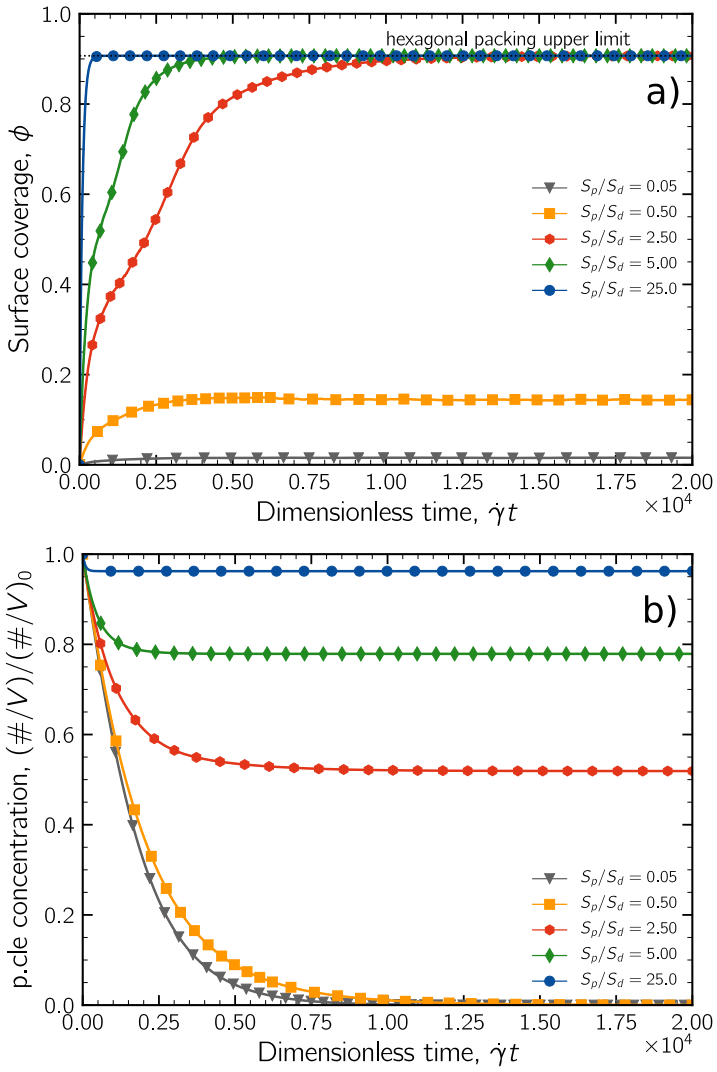

Figure 10: a) Temporal evolution of droplet population average coverage at varying initial ratio between the total particle surface S_p and the total droplet surface S_d. b) Temporal evolution of the concentration of free particles. The time scale has been made dimensionless in both plots by an equivalent shear rate $\dot{\gamma}$ computed as $\sqrt{\varepsilon/\nu}$, with ν being the water kinematic viscosity.

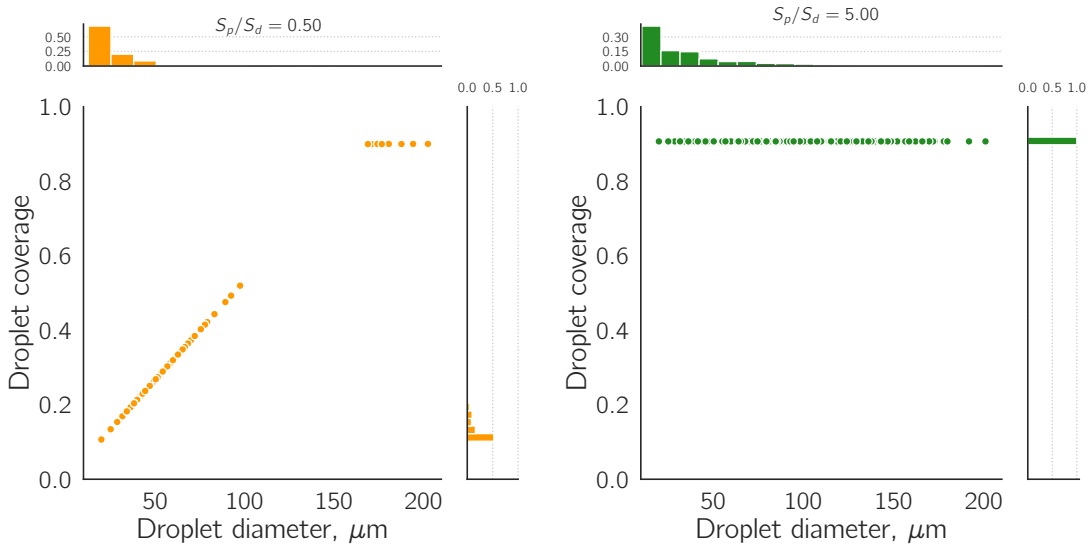

Figure 11: Bivariate distributions of the droplet size and coverage at varying particle content, expressed by the initial ratio between the total particle surface S_p and the total droplet surface S_d. The initial population was composed of droplets with zero surface coverage and diameter equal to 100μm.

the turbulent stresses. This effect was also present in the other investigated systems (see the distribution at $S_p/S_d = 5.00$), but here, given the larger amount of free particles initially dispersed, all droplets, including the smaller ones, presented the maximum attainable coverage at equilibrium.

Finally, we point out that the observed kinetics are determined by the specific choice of operative conditions and parameters used to model coalescence and breakup frequencies. However, we believe that the observed behavior are of general validity and should be expected to emerge during the transient of a turbulent emulsification process.

4. Conclusions

In this work we studied the dynamics of the flow-induced preparation of Pickering emulsions by means of a bivariate population balance model. We used established literature models for describing collision and breakup frequencies, whereas novel models for describing coalescence and breakup efficiencies were formulated. Both, the preparation in a uniform shear and in an isotropic turbulent flow were addressed. We assumed that, together with the coalescence and breakup phenomena of the droplet phase, coverage by solid particles also occurs, as determined by both the particle-droplet collisions induced by the velocity gradients of the flow and by the

particle Brownian motion. An event-driven Monte Carlo algorithm has been developed to solve the formulated population balance model.

Results shed light on the mechanism by which size stabilization is attained, and showed that the preparation of Pickering emulsions under fluid dynamic stresses is a process rich in phenomena, with a number of distinctive features affecting both the transient and the steady state conditions. Under shear, the steady state Sauter diameter of the droplets was found to scale inversely with the solid particle content, a result which qualitatively compares well with previously reported experiments. Results also showed that even low amount of dispersed particles can lead to fully stabilized emulsions. In this condition, we observed in fact coalescence to play a major role, together with particle adsorption, throughout the transient of the process, finally leading to the formation of large and highly covered droplets. At large particle concentrations, on the contrary, we observed at equilibrium smaller droplets whose size distribution became narrower and narrower as the amount of solid particles was increased.

Following recently reported data, we assumed that when droplets have a surface coverage larger than the percolation limit, they behave as *hard spheres* displaying an infinite resistance to the hydrodynamic stresses. Under this assumption, we observed size stabilization to occur in turbulence through a peculiar path: the droplet size was first reduced by the turbulent stresses, but as soon as the droplets became strong, they were possibly involved only in coalescence events. This finally led to both a distinctive dynamics in the droplet size, which presented an undershoot during the transient state, and in the equilibrium distributions, in which we observed small droplets coexisting with few large and fully covered droplets resisting turbulent breakup.

The results herein reported offer a wide view over the dynamics of Pickering emulsions processing in a fluid flow and, as such, we believe that they can be conveniently used to select formulation and fluid dynamic conditions to obtain emulsions with a precise dynamics of preparation and tuned properties. Furthermore, we believe that the emergence of a number of distinctive features in the transient of the process can be of use to possibly track and predict the outcome of the preparation. In this context, we also envision the modulation of the feeding profile of the particles as a possible strategy for the process control.

Mostly motivated by the scarce literature about the topic, we adopted a few assumptions (e.g., the threshold values of coverage for the suppression of coalescence and breakup, daughter droplets size distribution upon breakup) and working hypotheses (such as solid particle monodispersity, particle stability against aggregation, hexagonal packing, initial droplets properties). All are in need to be verified when interpreting the results of experimental tests and

can be relaxed in our model, if new experimental or numerical insights become available.

Finally, we focused our work on the study of two uniform flow conditions, namely laminar shear and homogeneous and isotropic turbulence. This choice is justified by the fact that, in common process equipment, at least at the scale of the droplets, such flow conditions hold. However, when the flow field has spatial inhomogeneities that are in need to be modeled (as may happen in stirred tanks, static mixers, or cone-mill devices), a characterization by computational fluid dynamics or by an experimental study can be used for a *compartmentalization* of the present model, i.e., different subvolumes, each with its own uniform fluid dynamics properties and rate of mass exchange with the surroundings, can be identified, and the overall population dynamics followed in the whole equipment.

Acknowledgments

Support from the "TUM Global Postdoc Fellowship" program, within which the present research has been conducted, is gratefully acknowledged.

References

Alopaeus, V., Koskinen, J., Keskinen, K. I., & Majander, J. (2002). Simulation of the population balances for liquid–liquid systems in a nonideal stirred tank. Part 2 – Parameter fitting and the use of the multiblock model for dense dispersions. *Chemical Engineering Science*, *57*, 1815–1825. doi:https://doi.org/10.1016/S0009-2509(02)00067-2.

Arditty, S., Whitby, C. P., Binks, B. P., Schmitt, V., & Leal-Calderon, F. (2003). Some general features of limited coalescence in solid-stabilized emulsions. *The European Physical Journal E*, *11*, 273–281. doi:https://doi.org/10.1140/epje/i2003-10018-6.

Aveyard, R., Binks, B. P., & Clint, J. H. (2003). Emulsions stabilised solely by colloidal particles. *Advances in Colloid and Interface Science*, *100*, 503–546. doi:https://doi.org/10.1016/S0001-8686(02)00069-6.

Binks, B. P. (2002). Particles as surfactants–similarities and differences. *Current opinion in Colloid & Interface science*, *7*, 21–41. doi:https://doi.org/10.1016/S1359-0294(02)00008-0.

Binks, B. P., & Lumsdon, S. O. (2000). Influence of particle wettability on the type and stability of surfactant-free emulsions. *Langmuir*, *16*, 8622–8631. doi:https://doi.org/10.1021/la000189s.

Briesen, H. (2006). Simulation of crystal size and shape by means of a reduced two-dimensional population balance model. *Chemical Engineering Science*, *61*, 104–112. doi:https://doi.org/10.1016/j.ces.2004.11.062.

Chang, F., Vis, C. M., Ciptonugroho, W., & Bruijnincx, P. C. (2021). Recent developments in catalysis with Pickering emulsions. *Green Chemistry*, *23*, 2575–2594. doi:https://doi.org/10.1039/D0GC03604H.

Chaturbedi, A., Pathak, C., Deshpande, K., Shapley, N., & Ramachandran, R. (2016). Population balance model development and experimental validation for the heteroaggregation of oppositely charged micro and nano-particles. *Chemical Engineering Research and Design*, *113*, 96–111. doi:https://doi.org/10.1016/j.cherd.2016.07.004.

Coulaloglou, C. A., & Tavlarides, L. L. (1977). Description of interaction processes in agitated liquid-liquid dispersions. *Chemical Engineering Science*, *32*, 1289–1297. doi:https://doi.org/10.1016/0009-2509(77)85023-9.

Debruijn, R. A. (1991). Deformation and breakup of drops in simple shear flows. *Ph. D. thesis*, *Technische Universiteit Eindhoven*. doi:https://doi.org/10.6100/IR318702.

Fan, H., & Striolo, A. (2012). Mechanistic study of droplets coalescence in Pickering emulsions. *Soft Matter*, *8*, 9533–9538. doi:https://doi.org/10.1039/C2SM26416A.

Ferrari, M., Handgraaf, J.-W., Boccardo, G., Buffo, A., Vanni, M., & Marchisio, D. L. (2022). Molecular modeling of the interface of an egg yolk protein-based emulsion. *Physics of Fluids*, *34*, 021903. doi:https://doi.org/10.1063/5.0079883.

Frijters, S., Günther, F., & Harting, J. (2014). Domain and droplet sizes in emulsions stabilized by colloidal particles. *Physical Review E*, *90*, 042307. doi:https://doi.org/10.1103/PhysRevE.90.042307.

Frungieri, G., Bäbler, M. U., & Vanni, M. (2020a). Shear-induced heteroaggregation of oppositely charged colloidal particles. *Langmuir*, *36*, 10739–10749. doi:https://doi.org/10.1021/acs.langmuir.0c01536.

Frungieri, G., Boccardo, G., Buffo, A., Karimi-Varzaneh, H. A., & Vanni, M. (2022a). CFD-DEM characterization and population balance modelling of a dispersive mixing process. *Chemical Engineering Science*, *260*, 117859. doi:https://doi.org/10.1016/j.ces.2022.117859.

Frungieri, G., Boccardo, G., Buffo, A., Marchisio, D., Karimi-Varzaneh, H. A., & Vanni, M. (2020b). A CFD-DEM approach to study the breakup of fractal agglomerates in an internal mixer. *The Canadian Journal of Chemical Engineering*, *98*, 1880–1892. doi:https://doi.org/10.1002/cjce.23773.

Frungieri, G., Carone, M., Riggio, V., Buffo, A., Vanni, M., & Zanetti, M. (2022b). Numerical modelling of a lab-scale reactor for microalgae growth. *Chemical Engineering Transactions*, *92*, 127–132. doi:https://doi.org/10.3303/CET2292022.

Frungieri, G., & Vanni, M. (2017). Shear-induced aggregation of colloidal particles: A comparison between two different approaches to the modelling of colloidal interactions. *The Canadian Journal of Chemical Engineering*, *95*, 1768–1780. doi:https://doi.org/10.1002/cjce.22843.

Frungieri, G., & Vanni, M. (2021). Aggregation and breakup of colloidal particle aggregates in shear flow: A combined Monte Carlo-Stokesian dynamics approach. *Powder Technology*, *388*, 357–370. doi:https://doi.org/10.1016/j.powtec.2021.04.076.

Gai, Y., Kim, M., Pan, M., & Tang, S. K. (2017). Amphiphilic nanoparticles suppress droplet break-up in a concentrated emulsion flowing through a narrow constriction. *Biomicrofluidics*, *11*, 034117. doi:https://doi.org/10.1063/1.4985158.

Ge, S., Agbakpe, M., Zhang, W., & Kuang, L. (2015). Heteroaggregation between PEI-coated magnetic nanoparticles and algae: effect of particle size on algal harvesting efficiency. *ACS Applied Materials & Interfaces*, *7*, 6102–6108. doi:https://doi.org/10.1021/acsami.5b00572.

Grace, H. P. (1982). Dispersion phenomena in high viscosity immiscible fluid systems and application of static mixers as dispersion devices in such systems. *Chemical Engineering Communications*, *14*, 225–277. doi:https://doi.org/10.1080/00986448208911047.

Guo, J., Cui, L., Huang, Y., & Meng, Z. (2022). Spirulina platensis protein isolate nanoparticle stabilized O/W Pickering emulsions: Interfacial adsorption and bulk aggregation. *Food Research International*, *161*, 111815. doi:https://doi.org/10.1016/j.foodres.2022.111815.

Hajisharifi, A., Marchioli, C., & Soldati, A. (2021). Particle capture by drops in turbulent flow. *Physical Review Fluids*, *6*, 024303. doi:https://doi.org/10.1103/PhysRevFluids.6.024303.

Hajisharifi, A., Marchioli, C., & Soldati, A. (2022). Interface topology and evolution of particle patterns on deformable drops in turbulence. *Journal of Fluid Mechanics*, *933*, A41. doi:https://doi.org/10.1017/jfm.2021.1094.

Jing, X., Chen, B., Liu, T., Cai, Y., Zhao, Q., Deng, X., & Zhao, M. (2022). Formation and stability of Pickering emulsion gels by insoluble soy peptide aggregates through hydrophobic modification. *Food Chemistry*, *387*, 132897. doi:https://doi.org/10.1016/j.foodchem.2022.132897.

Kempin, M. V., Kraume, M., & Drews, A. (2020). W/O Pickering emulsion preparation using a batch rotor-stator mixer – influence on rheology, drop size distribution and filtration behavior. *Journal of Colloid and Interface Science*, *573*, 135–149. doi:https://doi.org/10.1016/j.jcis.2020.03.103.

Kendall, D. G. (1949). Stochastic processes and population growth. *Journal of the Royal Statistical Society. Series B (Methodological)*, *11*, 230–282. doi:https://doi.org/10.1111/j.2517-6161.1949.tb00032.x.

Kuhn, M., Kirse, C., & Briesen, H. (2018). Population balance modeling and opinion dynamics – A mutually beneficial liaison? *Processes*, *6*, 164. doi:https://doi.org/10.3390/pr6090164.

Lebaz, N., Azizi, F., & Sheibat-Othman, N. (2021). Modeling droplet breakage in continuous emulsification using static mixers in the framework of the entire spectrum of turbulent energy. *Industrial & Engineering Chemistry Research*, *61*, 541–553. doi:https://doi.org/10.1021/acs.iecr.1c03529.

Lee, K., & Matsoukas, T. (2000). Simultaneous coagulation and break-up using constant-N Monte Carlo. *Powder Technology*, *110*, 82–89. doi:https://doi.org/10.1016/S0032-5910(99)00270-3.

Liffman, K. (1992). A direct simulation Monte-Carlo method for cluster coagulation. *J. Comput. Phys.*, *100*, 116–127. doi:https://doi.org/10.1016/0021-9991(92)90314-O.

López-Pedrouso, M., Lorenzo, J. M., Moreira, R., & Franco, D. (2022). Potential applications of Pickering emulsions and high internal phase emulsions (HIPEs) stabilized by starch particles. *Current Opinion in Food Science*, *46*, 100866. doi:https://doi.org/10.1016/j.cofs.2022.100866.

Low, L. E., Siva, S. P., Ho, Y. K., Chan, E. S., & Tey, B. T. (2020). Recent advances of characterization techniques for the formation, physical properties and stability of Pickering emulsion. *Advances in Colloid and Interface science*, *277*, 102117. doi:https://doi.org/10.1016/j.cis.2020.102117.

Luo, Z. Y., & Bai, B. F. (2020). Retardation of droplet transport in confined microchannel by interfacial jamming of nanoparticles. *Physics of Fluids*, *32*, 087110. doi:https://doi.org/10.1063/5.0016450.

Lv, S., Zhou, H., Bai, L., Rojas, O. J., & McClements, D. J. (2021). Development of food-grade Pickering emulsions stabilized by a mixture of cellulose nanofibrils and nanochitin. *Food Hydrocolloids*, *113*, 106451. doi:https://doi.org/10.1016/j.foodhyd.2020.106451.

Maisels, A., Kruis, F. E., & Fissan, H. (2004). Direct simulation Monte Carlo for simultaneous nucleation, coagulation, and surface growth in dispersed systems. *Chemical Engineering Science*, *59*, 2231–2239. doi:https://doi.org/10.1016/j.ces.2004.02.015.

Maluta, F., Alberini, F., Montante, G., & Paglianti, A. (2022). Validation of a procedure for the numerical simulations of gas–liquid stirred tanks by means of a computational fluid dynamics approach. *The Canadian Journal of Chemical Engineering*, *100*, 3472–3485. doi:https://doi.org/10.1002/cjce.24548.

Maluta, F., Buffo, A., Marchisio, D., Montante, G., Paglianti, A., & Vanni, M. (2021). Effect of turbulent kinetic energy dissipation rate on the prediction of droplet size distribution in stirred tanks. *International Journal of Multiphase Flow*, *136*, 103547. doi:https://doi.org/10.1016/j.ijmultiphaseflow.2020.103547.

Mei, Y., Li, G., Moldenaers, P., & Cardinaels, R. (2016). Dynamics of particle-covered droplets in shear flow: Unusual breakup and deformation hysteresis. *Soft matter*, *12*, 9407–9412. doi:https://doi.org/10.1039/C6SM02031C.

Ngai, T., & Bon, S. A. F. (2014). *Particle-stabilized emulsions and colloids: formation and applications*. Royal Society of Chemistry, Cambridge, UK.

Niño, L., Gelves, R., Ali, H., Solsvik, J., & Jakobsen, H. (2020). Applicability of a modified breakage and coalescence model based on the complete turbulence spectrum concept for CFD simulation of gas-liquid mass transfer in a stirred tank reactor. *Chemical Engineering Science*, *211*, 115272. doi:https://doi.org/10.1016/j.ces.2019.115272.

Para, M. L., Alidoost, M., Shiea, M., Boccardo, G., Buffo, A., Barresi, A. A., & Marchisio, D. (2022). A modelling and experimental study on the co-precipitation of $Ni_{0.8}Mn_{0.1}Co_{0.1}(OH)_2$ as precursor for battery cathodes. *Chemical Engineering Science*, *254*, 117634. doi:https://doi.org/10.1016/j.ces.2022.117634.

Pawar, A. B., Caggioni, M., Ergun, R., Hartel, R. W., & Spicer, P. T. (2011). Arrested coalescence in Pickering emulsions. *Soft Matter*, *7*, 7710–7716. doi:https://doi.org/10.1039/C1SM05457K.

Pickering, S. U. (1907). CXCVI–Emulsions. *Journal of the Chemical Society, Transactions*, *91*, 2001–2021. doi:https://doi.org/10.1039/CT9079102001.

Ramsden, W. (1904). Separation of solids in the surface-layers of solutions and suspensions (observations on surface-membranes, bubbles, emulsions, and mechanical coagulation).– Preliminary account. *Proceedings of the Royal Society of London*, *72*, 156–164. doi:https://doi.org/10.1098/rspl.1903.0034.

Rhein, F., Ruß, F., & Nirschl, H. (2019). Collision case model for population balance equations in agglomerating heterogeneous colloidal systems: Theory and experiment. *Colloids and Surfaces A: Physicochemical and Engineering Aspects*, *572*, 67–78. doi:https://doi.org/10.1016/j.colsurfa.2019.03.089.

Rollié, S., Briesen, H., & Sundmacher, K. (2009). Discrete bivariate population balance modelling of heteroaggregation processes. *Journal of Colloid and Interface Science*, *336*, 551–564. doi:https://doi.org/10.1016/j.jcis.2009.04.031.

Schmideder, S., Kirse, C., Hofinger, J., Rollié, S., & Briesen, H. (2018). Modeling the separation of microorganisms in bioprocesses by flotation. *Processes*, *6*, 184. doi:https://doi.org/10.3390/pr6100184.

Shah, B. H., Ramkrishna, D., & Borwanker, J. D. (1977). Simulation of particulate systems using the concept of the interval of quiescence. *AIChE Journal*, *23*, 897–904. doi:https://doi.org/10.1002/aic.690230617.

Sharkawy, A., Silva, A. M., Rodrigues, F., Barreiro, F., & Rodrigues, A. (2021). Pickering emulsions stabilized with chitosan/collagen peptides nanoparticles as green topical delivery vehicles for cannabidiol (CBD). *Colloids and Surfaces A: Physicochemical and Engineering Aspects*, *631*, 127677. doi:https://doi.org/10.1016/j.colsurfa.2021.127677.

Singh, M., Ranade, V., Shardt, O., & Matsoukas, T. (2022). Challenges and opportunities concerning numerical solutions for population balances: A critical review. *Journal of Physics A: Mathematical and Theoretical*, *55*, 383002. doi:https://doi.org/10.1088/1751-8121/ac8a42.

Siva, S. P., & Ho, Y. K. (2022). Modeling the adsorption of polydispersed cellulose nanocrystals on emulsion oil droplets during their simultaneous breakage and coalescence. *Industrial & Engineering Chemistry Research*, *61*, 3983–4000. doi:https://doi.org/10.1021/acs.iecr.1c03946.

Smoluchowski, M. V. (1918). Versuch einer mathematischen Theorie der Koagulationskinetik kolloider Lösungen. *Zeitschrift für physikalische Chemie*, *92*, 129–168. doi:https://doi.org/10.1515/zpch-1918-9209.

Solsvik, J., Becker, P. J., Sheibat-Othman, N., & Jakobsen, H. A. (2014). Population balance model: Breakage kernel parameter estimation to emulsification data. *The Canadian Journal of Chemical Engineering*, *92*, 1082–1099. doi:https://doi.org/10.1002/cjce.21928.

Solsvik, J., Tangen, S., & Jakobsen, H. A. (2013). On the constitutive equations for fluid particle breakage. *Reviews in Chemical Engineering*, *29*, 241–356. doi:https://doi.org/10.1515/revce-2013-0009.

Tsabet, E., & Fradette, L. (2015). Effect of processing parameters on the production of Pickering emulsions. *Industrial & Engineering Chemistry Research*, *54*, 2227–2236. doi:https://doi.org/10.1021/ie504338d.

Vasquez Giuliano, L., Buffo, A., Vanni, M., & Frungieri, G. (2022a). Micromechanics and strength of agglomerates produced by spray drying. *JCIS Open*, *in press*. doi:https://doi.org/10.1016/j.jciso.2022.100068.

Vasquez Giuliano, L., Buffo, A., Vanni, M., Lanotte, A. S., Arima, V., Bianco, M., Baldassarre, F., & Frungieri, G. (2022b). Response of shear-activated nanotherapeutic particles in a clot-obstructed blood vessel by CFD-DEM simulations. *The Canadian Journal of Chemical Engineering*, *100*, 3562–3574. doi:https://doi.org/10.1002/cjce.24502.

Voisin, H., Falourd, X., Rivard, C., & Capron, I. (2021). Versatile nanocellulose-anatase TiO_2 hybrid nanoparticles in Pickering emulsions for the photocatalytic degradation of organic

and aqueous dyes. *JCIS Open*, *3*, 100014. doi:https://doi.org/10.1016/j.jciso.2021.100014.

Wang, J., Sun, Y., Yu, M., Lu, X., Komarneni, S., & Yang, C. (2021). Emulsions stabilized by highly hydrophilic TiO_2 nanoparticles via van der Waals attraction. *Journal of Colloid and Interface Science*, *589*, 378–387. doi:https://doi.org/10.1016/j.jcis.2021.01.011.

Wiley, R. M. (1954). Limited coalescence of oil droplets in coarse oil-in-water emulsions. *Journal of Colloid Science*, *9*, 427–437. doi:https://doi.org/10.1016/0095-8522(54)90030-6.

Zhang, X., Hou, Y., Ettelaie, R., Guan, R., Zhang, M., Zhang, Y., & Yang, H. (2019). Pickering emulsion-derived liquid–solid hybrid catalyst for bridging homogeneous and heterogeneous catalysis. *Journal of the American Chemical Society*, *141*, 5220–5230. doi:https://doi.org/10.1021/jacs.8b11860.

Zhao, H., Li, J., Wang, L., Li, C., & Zhang, S. (2021). Pickering emulsion stabilized by dual stabilizer: A novel reaction/separation system for methacrolein synthesis. *Chemical Engineering Science*, *229*, 116038. doi:https://doi.org/10.1016/j.ces.2020.116038.

Zhao, W., Jama, M. A., Buffo, A., & Alopaeus, V. (2018). Population balance model and experimental validation for reactive dissolution of particle agglomerates. *Computers & Chemical Engineering*, *108*, 240–249. doi:https://doi.org/10.1016/j.compchemeng.2017.09.019.